INTERNATIONAL JOURNAL FOR NUMERICAL METHODS IN FLUIDS, VOL. 11, 1–20 (1990)

# EVALUATION OF A COUPLED SOLUTION APPROACH FOR FLUID FLOW CALCULATIONS IN BODY-FITTED CO-ORDINATES

K. C. KARKI AND H. C. MONGIA

*Allison Gas Turbine Division, General Motors Corporation, Indianapolis, IN 46206-0420, U.S.A.*

## SUMMARY

An investigation has been conducted to study the performance of a coupled solution approach for solving the fluid flow equations in body-fitted co-ordinates using a covariant velocity formulation. The set of discrete equations is solved using a sparse matrix variant of LU decomposition. A series of test problems have been considered to study the effects of Reynolds number, mesh skewness and grid size on the convergence rate. The coupled solution approach has been compared with a state-of-the-art sequential approach. The results indicate that the coupled technique is faster by a factor of about two for reasonable grids. For severely non-orthogonal grids the performance of the coupled solution approach deteriorates considerably.

KEY WORDS Curvilinear co-ordinates Coupled solution Viscous flows SIMPLER algorithm

## INTRODUCTION

In the primitive variable discrete formulation of the incompressible Navier–Stokes equations, the treatment of the velocity–pressure coupling has a major influence on the convergence characteristics of the calculation procedure. A most successful approach for handling the velocity–pressure coupling is the SIMPLE algorithm.[1,2] In this method the continuity and momentum equations are combined to obtain an equation for pressure correction, and the equations are solved in a decoupled manner. Briefly, the sequence of calculations is as follows. The momentum equations are solved with a guessed pressure field. This is followed by the solution of the pressure correction equation. These corrections are used to update the existing pressure and velocity fields. The linearized algebraic equations are usually solved using a line relaxation method. In recent years, various improved variants of SIMPLE have been suggested, including SIMPLER,[2,3] SIMPLEC[4] and PISO.[5]

An alternative to the sequential approach is to solve the Navier–Stokes equations in a fully coupled manner.[6–9] The discretized continuity and momentum equations are assembled into one large set and solved using a sparse variant of LU decomposition. The resulting algorithm has been shown to be rapidly convergent and robust to changes in Reynolds number, grid aspect ratio and number of grid points. For flows in simple geometries using Cartesian and cylindrical co-ordinates, the coupled solution approach has been shown to be significantly faster than the SIMPLE algorithm. The only major drawback of the sparse matrix procedure is the large amount of computer storage. Some techniques to alleviate this problem have been suggested in Reference 7.

0271–2091/90/090001–20$10.00

*Received 3 June 1988*
*Revised 5 October 1988*

With the increasing popularity of the finite difference (volume) techniques for computing flows in complex geometries, it is of importance to evaluate the performance of the coupled solution algorithms in a generalized curvilinear co-ordinate system. The use of non-orthogonal curvilinear co-ordinates adds several complexities in the overall calculation procedure. These arise, for example, from the presence of the diffusion terms involving cross-derivatives, additional pressure gradient terms, and the 'curvature' source terms if the non-Cartesian velocity components are used as the dependent variables. Since there are various options available for the grid arrangement and the dependent variables, the performance of a solution algorithm will depend on the particular formulation used.

In Reference 10 the coupled solution technique has been used in conjunction with a Cartesian velocity formulation for fluid flow calculations in body-fitted co-ordinates. It was found that even though the coupled solution approach exhibited a superior rate of convergence, it was not as cost-effective as the iterative SIMPLE-based approach, especially for recirculating flows.

In the Cartesian velocity formulation adopted in Reference 10 a staggered grid arrangement is used and one velocity component is stored at each control volume face. Such a practice leads to simple conservation equations. However, the applicability of the method is dependent on the orientation of the grid lines relative to the reference Cartesian co-ordinate system. A more robust calculation procedure can be developed by using the covariant or the contravariant components of velocity as the dependent variables in the momentum equations. Since these velocity components tend to follow the grid lines, there are no limitations regarding the orientation of the computational grid.

In the present paper a coupled solution technique has been employed to solve the Navier–Stokes equations in a body-conforming co-ordinate system. Following References 11 and 12, the velocity components along the co-ordinate lines (covariant components) are selected as the primary variables. The performance of the resulting algorithm has been contrasted with that of a sequential approach based on the SIMPLER algorithm. A series of test problems have been considered and the effects of Reynolds number, grid size and mesh skewness on the convergence behaviour have been presented.

## DERIVATION OF THE DISCRETE EQUATIONS OF MOTION

### *Differential equations*

The conservation equation for a dependent variable $\phi$ in a generalized co-ordinate system $(\xi, \eta)$ can be written as

$$\frac{1}{J}\frac{\partial}{\partial \xi}(\rho U \phi)+\frac{1}{J}\frac{\partial}{\partial \eta}(\rho V \phi)=\frac{1}{J}\frac{\partial}{\partial \xi}\left[\frac{\Gamma}{J}\left(c_1\frac{\partial \phi}{\partial \xi}-c_2\frac{\partial \phi}{\partial \eta}\right)\right]+\frac{1}{J}\frac{\partial}{\partial \eta}\left[\frac{\Gamma}{J}\left(c_3\frac{\partial \phi}{\partial \eta}-c_2\frac{\partial \phi}{\partial \xi}\right)\right]+S, \tag{1a}$$

where

$$U = u\frac{\partial y}{\partial \eta}-v\frac{\partial x}{\partial \eta}, \tag{1b}$$

$$V = v\frac{\partial x}{\partial \xi}-u\frac{\partial y}{\partial \xi}, \tag{1c}$$

$$c_1=\left(\frac{\partial x}{\partial \eta}\right)^2+\left(\frac{\partial y}{\partial \eta}\right)^2, \tag{1d}$$

$$c_2 = \frac{\partial x}{\partial \xi}\frac{\partial x}{\partial \eta} + \frac{\partial y}{\partial \xi}\frac{\partial y}{\partial \eta}, \tag{1e}$$

$$c_3 = \left(\frac{\partial x}{\partial \xi}\right)^2 + \left(\frac{\partial y}{\partial \xi}\right)^2, \tag{1f}$$

$$J = \frac{\partial x}{\partial \xi}\frac{\partial y}{\partial \eta} - \frac{\partial y}{\partial \xi}\frac{\partial x}{\partial \eta}. \tag{1g}$$

In these equations $u$ and $v$ are Cartesian velocity components, $\Gamma$ is the diffusivity and $S(\xi, \eta)$ is the source of $\phi$ in the $(\xi, \eta)$ co-ordinates. For velocity components ($\phi = u, v$), $S$ also includes the corresponding pressure gradient term.

*Discretization equations*

The discretization is performed in the physical space following a finite volume approach in which the computational domain is divided into contiguous control volumes. A staggered grid arrangement is used in which the scalar quantities are located at the geometrical center of the control volume and the velocity components are displaced in the co-ordinate directions to lie at the midpoinds of the control volume faces. In the present work the physical covariant velocity components are chosen as the dependent variables. Similar to the practice followed in orthogonal co-ordinates, only one velocity component is stored at a control volume face. The locations of various dependent variables are shown in Figure 1.

The discretization equations for the covariant velocity components are obtained by combining the discretization equations for the Cartesian velocity components rather than integrating their

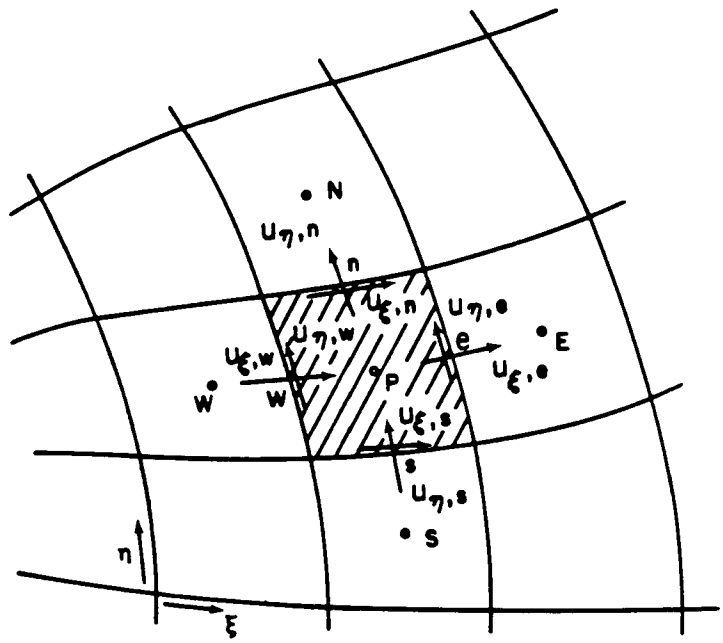


Figure 1. Location of various dependent variables

own differential equations. A brief description of the method is presented here; complete details are available in References 11 and 12.

For illustration purposes, the discretization equation for velocity component $u_{\xi,\,e}$ in Figure 1 is derived. The procedure is identical for other velocity components. The discretization equations for the Cartesian velocity components $u$ and $v$ located at 'e' can be written as

$$a_e u_e = \sum a_i u_i - \left( \frac{\partial y}{\partial \eta}\frac{\partial p}{\partial \xi} - \frac{\partial y}{\partial \xi}\frac{\partial p}{\partial \eta} \right) + b_u, \tag{2}$$

$$a_e v_e = \sum a_i v_i - \left( \frac{\partial x}{\partial \xi}\frac{\partial p}{\partial \eta} - \frac{\partial x}{\partial \eta}\frac{\partial p}{\partial \xi} \right) + b_v. \tag{3}$$

Note that since $u$ and $v$ are co-located, the coefficient $a_i$ is the same for both equations. In the present formulation the cross-diffusion terms involving $c_2$ in equation (1a) are calculated explicitly and treated as source terms. Further, the power-law differencing scheme[2, 3] has been emloyed to obtain the combined convection diffusion coefficients $a_i$. Such a practice leads to a five-point computational molecule in two dimensions. Thus the summation in equations (2) and (3) is over four neighbours of 'e'.

The covariant velocity component $u_{\xi,\,e}$ along the $\xi$-co-ordinate line is defined as

$$u_{\xi,\,e} = (\mathbf{V}\cdot\mathbf{e}_\xi)_e = \frac{(u\,\partial x/\partial\xi + v\,\partial y/\partial\xi)_e}{(c_3)_e^{1/2}}. \tag{4}$$

The discretization equation for $u_{\xi,\,e}$ is obtained by combining equations (2)–(4). The resulting equation can be written as

$$a_e u_{\xi,\,e} = \sum a_i \tilde{u}_{\xi,\,i} - E_e \left( \frac{\partial p}{\partial \xi} \right)_e + \tilde{b}_{u_\xi}, \tag{5a}$$

where

$$\tilde{u}_{\xi,\,i} = \mathbf{V}_i \cdot \mathbf{e}_{\xi,\,e}, \tag{5b}$$

$$E = \frac{J}{(c_3)^{1/2}}, \tag{5c}$$

$$\tilde{b}_{u_\xi} = \frac{b_u(\partial x/\partial\xi) + b_v(\partial v/\partial\xi)}{(c_3)^{1/2}}. \tag{5d}$$

In the above equations, all geometrical quantities now pertain to the control volume for the velocity component $u_{\xi,\,e}$. To obtain a five-point formulation, equation (5a) is rearranged as

$$a_e u_{\xi,\,e} = \sum a_i u_{\xi,\,i} + E_e(p_P - p_E) + b_{u_\xi}, \tag{6a}$$

where $u_{\xi,\,i}$ is the velocity component along the $\xi$-co-ordinate line at location $i$, defined as

$$u_{\xi,\,i} = (\mathbf{V}\cdot\mathbf{e}_\xi)_i, \tag{6b}$$

and

$$b_{u_\xi} = \tilde{b}_{u_\xi} + \sum a_i(\tilde{u}_{\xi,\,i} - u_{\xi,\,i}). \tag{6c}$$

The discretized continuity equation for the control volume around grid point P in Figure 1 is

$$(\rho U)_e - (\rho U)_w + (\rho V)_n - (\rho V)_s = 0. \tag{7}$$

The contravariant velocities $U$ and $V$ are related to $u_\xi$ and $u_\eta$ as follows:

$$U = \alpha_\xi u_\xi - \beta_\xi u_\eta, \tag{8a}$$

$$V = \alpha_\eta u_\eta - \beta_\eta u_\xi, \tag{8b}$$

where

$$\alpha_\xi = \frac{c_1}{J}(c_3)^{1/2}, \tag{8c}$$

$$\beta_\xi = \frac{c_2}{J}(c_1)^{1/2}, \tag{8d}$$

$$\alpha_\eta = \frac{c_3}{J}(c_1)^{1/2}, \tag{8e}$$

$$\beta_\eta = \frac{c_2}{J}(c_3)^{1/2}. \tag{8f}$$

## SOLUTION ALGORITHMS

*Sequential (iterative) approach*

In the sequential solution procedure the velocity–pressure coupling is handled by solving an equation for pressure or pressure correction which is obtained by combining the discretized continuity and momentum equations. In the present study the SIMPLER algorithm has been used. In this procedure the pressure field is obtained by solving a Poisson-like equation and the mass conservation is enforced via a pressure correction.

*Pressure correction equation*

Let $u_\xi^*$ and $u_\eta^*$ denote the velocities after the solution of the momentum equations based on an estimated pressure field $p^*$. In general, these velocity components will not satisfy the continuity equation. Therefore corrections to $p^*$ are sought such that the resulting corrections to the velocity field will ensure the conservation of mass. The velocity corrections are related to the pressure corrections using an approximate form of the momentum equations. For example, from equation (6a),

$$u'_{\xi,\,e} = u_{\xi,\,e} - u^*_{\xi,\,e} = \frac{E_e}{a_e}(p'_P - p'_E) = d_e(p'_P - p'_E), \tag{9}$$

where $u'_\xi$ and $p'$ are velocity and pressure corrections, respectively.

The mass flow rate at the east face of a control volume can be expressed in terms of $p'$ as follows:

$$(\rho U)_e = \rho_e \alpha_{\xi,\,e}(u^*_{\xi,\,e} + u'_{\xi,\,e}) - \rho_e \beta_{\xi,\,e} u^0_{\eta,\,e} \tag{10a}$$

or

$$(\rho U)_e = \rho_e \alpha_{\xi,\,e}[u^*_{\xi,\,e} + d_e(p'_P - p'_E)] - \rho_e \beta^0_{\xi,\,e} u_{\eta,\,e}. \tag{10b}$$

Similarly,

$$(\rho V)_n = \rho_n \alpha_{\eta,\,n}[u^*_{\eta,\,n} + d_n(p'_P - p'_N)] - \rho_n \beta_{\eta,\,n} u^0_{\xi,\,n}. \tag{11}$$

In the above equations, $u^0_{\eta,\,e}$ and $u^0_{\xi,\,n}$ are the velocity components along the east and north faces of the control volume respectively. These velocity components are obtained by averaging the covariant velocity components at the neighbouring locations and are treated explicitly. A fully implicit formulation which allows for corrections for these velocity components is also possible. The resulting pressure correction equation, however, becomes complicated. Such a formulation was not considered in this study.

The pressure correction equation is obtained by substituting the expressions for mass flow rates, e.g. equations (10) and (11), in the discretized continuity equation. The final equation can be expressed as

$$a_P p'_P = \sum a_i p'_i + b, \quad i = \mathrm{E, W, N, S}, \tag{12a}$$

where the coefficients $a_i$ are defined as

$$a_E = (\rho \alpha_\xi d)_e, \tag{12b}$$

$$a_W = (\rho \alpha_\xi d)_w, \tag{12c}$$

$$a_N = (\rho \alpha_n d)_n, \tag{12d}$$

$$a_S = (\rho \alpha_\eta d)_s, \tag{12e}$$

$$a_P = \sum a_i, \tag{12f}$$

$$b = \rho_w(\alpha_\xi u^*_\xi - \beta_\xi u^0_\eta)_w - \rho_e(\alpha_\xi u^*_\xi - \beta_\xi u^0_\eta)_e + \rho_s(\alpha_\eta u^*_\eta - \beta_\eta u^0_\xi)_s - \rho_n(\alpha_\eta u^*_\eta - \beta_\eta u^0_\xi)_n. \tag{12g}$$

In the derivation of the pressure correction equation the velocity components along the control volume faces are treated explicitly. To ensure that the continuity equation is implicitly satisfied, the pressure correction equation is solved a few (typically four) times by updating the explicit terms.

*Pressure equation*

The steps in the derivation of the pressure equation are similar to those for the $p'$-equation. Instead of the approximate form, the full momentum equations are now used. The expressions for mass flow rates, such as equations (10), are written in terms of pseudovelocities $\hat{u}_\xi$ and pressures as follows:

$$(\rho U)_e = \rho_e \alpha_{\xi,\,e}[\hat{U}_{\xi,\,e} + d_e(p_P - p_E)] - \rho_e \beta_{\xi,\,e} u^0_{\eta,\,e}, \tag{13a}$$

where

$$\hat{U}_{\xi,\,e} = \frac{\sum a_i U_{\xi,\,i} + b_{u_\xi}}{a_e}. \tag{13b}$$

The resulting pressure equation is very similar to the $p'$-equation. The starred velocities are now replaced by pseudovelocities and pressure $p$ takes the place of $p'$.

The sequence of steps in the SIMPLER algorithm is as follows.

1. Guess the velocity field.
2. Calculate the coefficients in the momentum equations and evaluate the pseudovelocities.
3. Solve the pressure equation.
4. With the known pressure field, solve the momentum equations to obtain $u^*_\xi$ and $u^*_\eta$.
5. Solve the pressure correction equation and correct the starred velocities.
6. Return to step 2 with the corrected velocity field and repeat the procedure until convergence.

*Coupled (direct) solution approach*

In the coupled solution procedure the discretized continuity and momentum equations are assembledinto a large set and solved in a fully coupled manner using a spare matrix form of LU decomposition. Since the velocities and pressures are simultaneously updated, the velocity–pressure coupling is implicitly retained. However, iterations are still necessary because of the non-linearities of convection terms and the explicit treatment of various source terms. In the present work the non-linearities in the equations were handled using the successive substitution (Picard) technique. The linearized equations take the form

$$\mathbf{A}\boldsymbol{\phi} = \mathbf{B}, \tag{14}$$

where $\boldsymbol{\phi} = [u_\xi, u_\eta, p]^T$, $\mathbf{A}$ is the coefficient matrix and $\mathbf{B}$ is the vector of source terms.

The structure of the coefficient matrix for the present formulation depends on the manner in which the secondary velocities appearing in the continuity equation are treated. If these velocity components are considered in an explicit manner, the coefficient matrix is identical to that encountered in a Cartesian co-ordinate system and is as shown in Figure 2(a). Alternatively, if all velocity components in the continuity equation are treated implicitly, the matrix structure shown in Figure 2(b) results. Owing to the presence of additional elements, the cost of factorizing the matrix increases considerably. Consequently, it was decided not to consider the continuity equation in a fully implicit manner.

As discussed earlier in the context of the sequential solution algorithm, an implicit satisfaction of the continuity equation is essential to ensure a good convergence rate. Owing to the explicit treatment of the velocities along the control volume faces, the velocity field following the coupled solution of the discrete continuity and momentum equations will in general not satisfy the continuity equation. Therefore a means of correcting this velocity field is needed. Here a pressure correction strategy similar to that in the sequential approach is used.

In the present study the Yale Sparse Matrix Package (YSMP)[13] is used for the LU decomposition. YSMP selects the elements of the main diagonal of the matrix as pivots during the decomposition process. Therefore it is necessary that the coefficient matrix does not contain any zero element on the main diagonal. As seen in Figure 2, the absence of pressure in the continuity equation leads to zeros along the main diagonal. This difficulty can be overcome in several ways, e.g. by rearranging the equations[6, 7] or by deriving an equation for pressure. In the present study, following References 8–10, small non-zero elements are introduced along the main diagonal in the continuity equation. To ensure that the resulting solution will satisfy the continuity equation correctly, equation (14) is recast in terms of an update vector as follows:

$$\mathbf{A}\Delta\boldsymbol{\phi} = \mathbf{B} - \mathbf{A}\boldsymbol{\phi}^*, \tag{15}$$

where $\Delta\boldsymbol{\phi} = \boldsymbol{\phi} - \boldsymbol{\phi}^*$ and $\boldsymbol{\phi}^*$ is the value from the previous iteration or initial guess. Now equation (15) is replaced by

$$\mathbf{A}'\Delta\boldsymbol{\phi} = \mathbf{B} - \mathbf{A}\boldsymbol{\phi}^*, \tag{16}$$

where $\mathbf{A}'$ is the perturbed matrix that contains small non-zero elements along the main diagonal. Since $\mathbf{A}'$ is not used on the right-hand side, the converged solution of equation (16) represents the solution of equation (14) with the continuity equation properly satisfied. An added advantage of solving the equations in terms of the changes is that it reduces the computer round-off errors.

Since the repeated numeric factorization of the coefficient matrix $\mathbf{A}$ is an expensive process, considerable execution time can be saved by freezing the coefficient matrix after the solution is near convergence. Thus, the coefficient matrix is not factorized at each iteration. Instead, the

factorized matrix from the previous iteration is used. In effect, equation (16) is replaced by

$$\mathbf{A}^*\Delta\boldsymbol{\phi} = \mathbf{B} - \mathbf{A}\boldsymbol{\phi}^*, \tag{17}$$

where $\mathbf{A}^*$ is the old matrix factorized at an earlier iteration but $\mathbf{A}$ is the current coefficient matrix. Thus, after the factorized matrix is frozen, the right-hand side is updated and the solution is obtained by forward and backward substitution using the know factorization of $\mathbf{A}$. The cost of one such iteration is only 5%–10% of a full factorization iteration.

## TEST PROBLEMS

The sequential and coupled solution procedures were applied to two test problems—(1) a wall-driven sheared cavity and (2) a planar curved channel. For the sheared cavity shown in Figure 3(a), the angle was varied with fixed values of $H = L = 1$. For the curved channel, the contours of the walls are prescribed as parabolic functions of the form

$$y = A + Bx^2, \quad 0 \leqslant x \leqslant 1 \tag{18}$$

The inlet height of the channel was fixed at 0·2. Two values of the parameter $B$ were used, namely $B = 0{\cdot}8$ and $1{\cdot}1$. These configurations are shown in Figures 3(b) and 3(c) respectively.

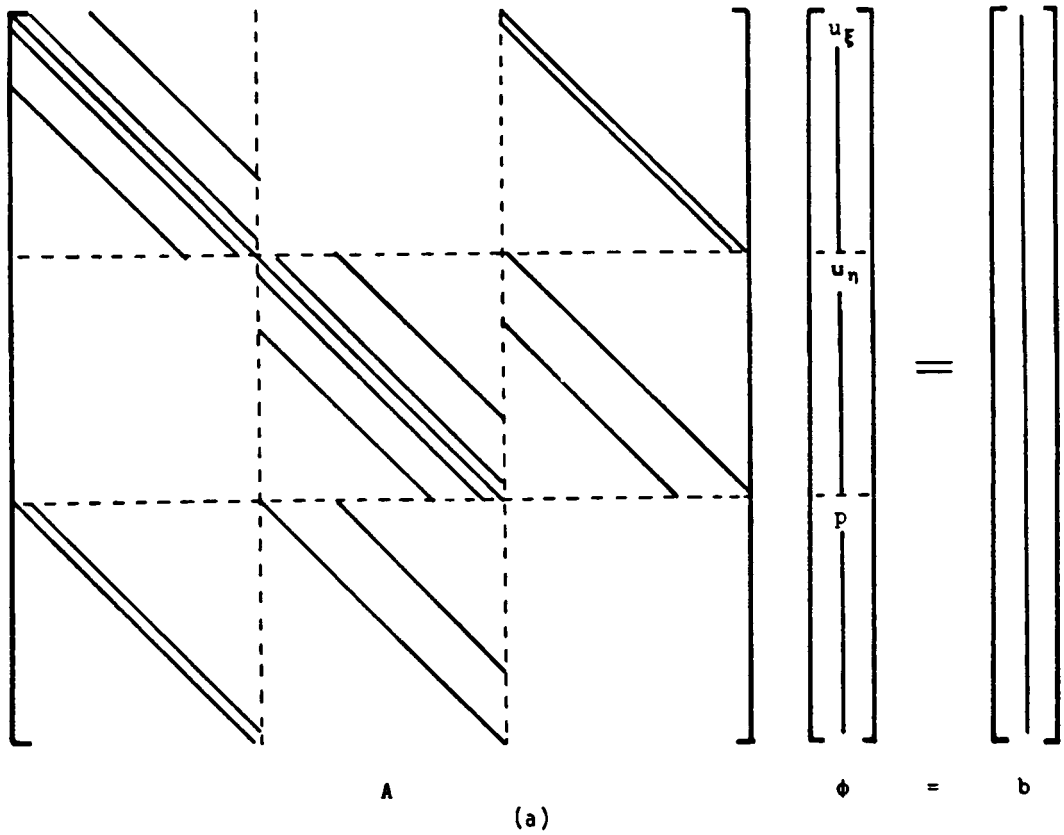


Figure 2(a)

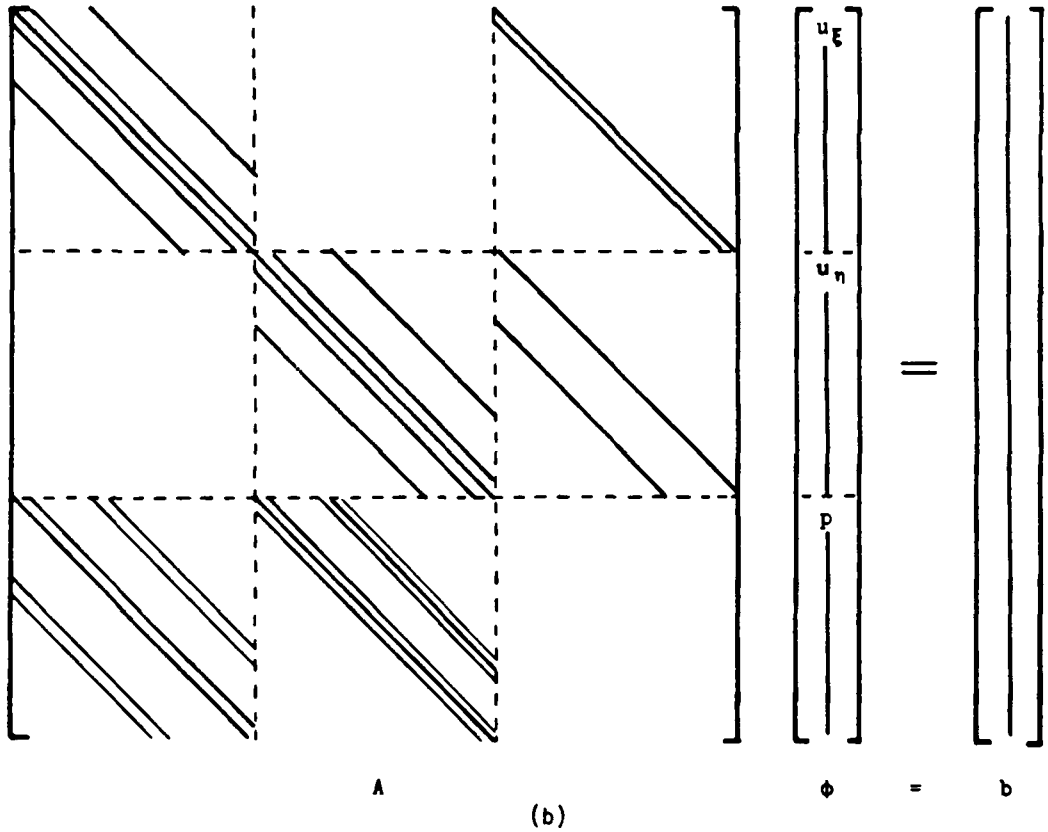


Figure 2. Structure of the coefficient matrix: (a) with explicit terms in the continuity equation; (b) with fully implicit continuity equation

Only laminar flows were investigated in this study. The majority of the results presented are for the sheared cavity. The channel case is similar to that used in Reference 10 and allows a comparison of the convergence behaviour of two alternative formulations for body-fitted co-ordinates. A parametric study with grid skewness, Reynolds number and grid spacing has been performed. All test cases considered in this study are listed in Table I.

## RESULTS

In this section the convergence characteristics of the two solution algorithms are compared. In the sequential solution approach the equations are solved using a line tridiagonal matrix algorithm (TDMA) supplemented by a block correction procedure.[3] A residual reduction criterion was used to terminate the number of TDMA sweeps. An underrelaxation factor of 0·7 was used for the velocity components; pressure and pressure correction were not underrelaxed. The pressure correction equation was solved four times by updating the right-hand side.

In the coupled solution procedure, no underrelaxation was required for any variable. The pressure correction equation was again solved four times. The factorization of the coefficient matrix was frozen after five iterations for the sheared cavity flows and after three iterations for the non-separating curved channel flows.

For each test case the absolute sums of the residuals of the continuity and $u_\xi$ (UKSI) momentum equations in all control volumes, normalized by reference values, are used to characterize the convergence rates. In the figures to follow, the sequential approach has been designated as 'S' and the coupled approach as 'C'.

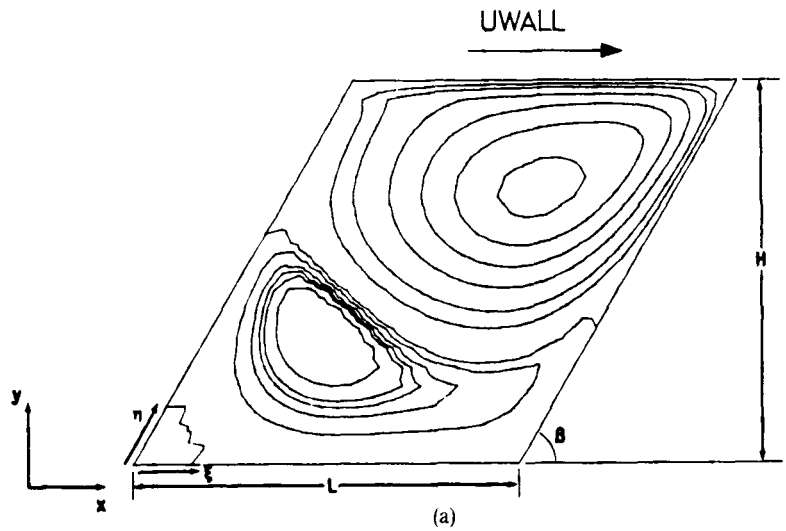


(a)

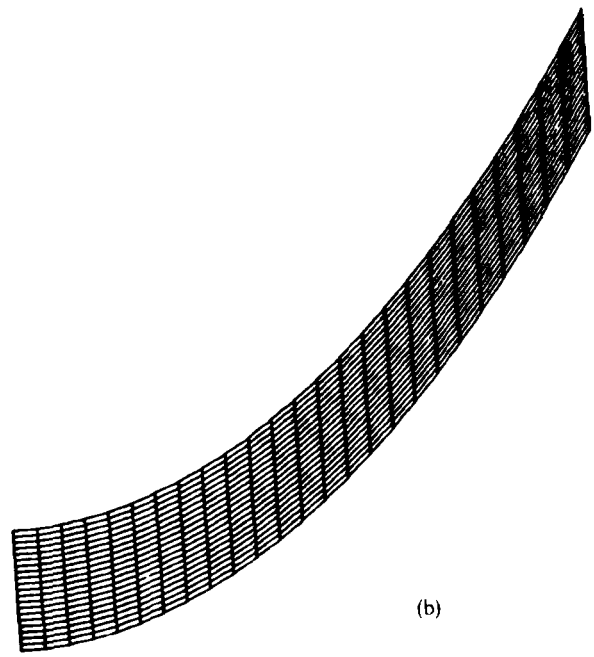

(b)

Figure 3(a, b)

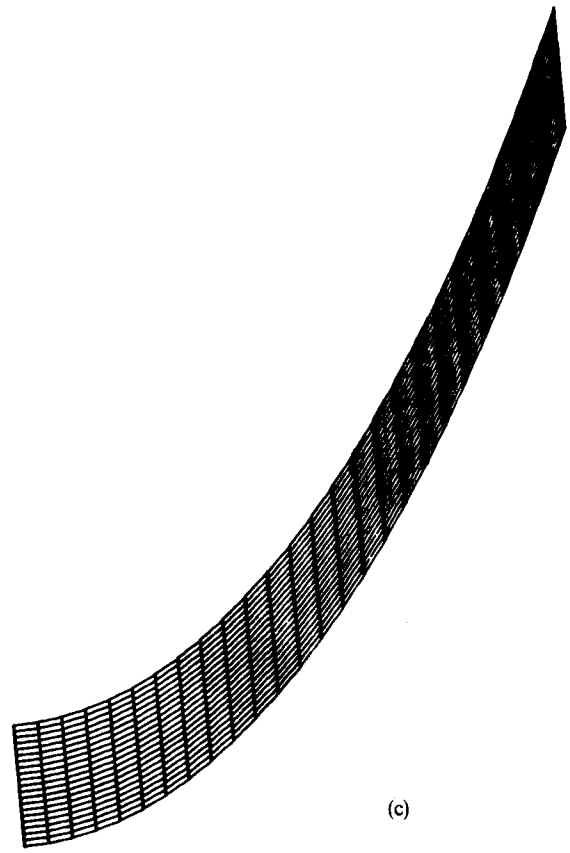


Figure 3. Test cases: (a) sheared cavity; (b) planar channel, $B = 0{\cdot}8$; (c) planar channel, $B = 1{\cdot}1$

Table I. Test cases considered

| Test case | Flow description | Grid |
|---|---|---|
| 1 | Sheared cavity, $Re = 400$, $\beta = 60°$ | 22 × 22 |
| 2 | Sheared cavity, $Re = 400$, $\beta = 45°$ | 22 × 22 |
| 3 | Sheared cavity, $Re = 1000$, $\beta = 60°$ | 22 × 22 |
| 4 | Sheared cavity, $Re = 1000$, $\beta = 45°$ | 22 × 22 |
| 5 | Sheared cavity, $Re = 1000$, $\beta = 45°$ | 32 × 32 |
| 6 | Planar channel, $Re = 2000$, $B = 0{\cdot}8$ | 27 × 22 |
| 7 | Planar channel, $Re = 2000$, $B = 1{\cdot}1$ (grid shown in Figure 3(c)) | 27 × 22 |
| 8 | Planar channel, $Re = 2000$, $B = 0{\cdot}8$ | 42 × 22 |
| 9 | Planar channel, $Re = 2000$, $B = 1{\cdot}1$ | 42 × 22 |
| 10 | Planar channel, $Re = 2000$, $B = 1{\cdot}1$ (grid shown in Figure 10) | 42 × 22 |

*Sheared cavity*

The computations for the sheared cavity were made on a uniformly spaced sheared grid in which the co-ordinate lines are parallel to the walls of the cavity. Figure 4 shows the convergence rates of the sequential and the coupled solution algorithms at a Reynolds number, based on the lid velocity and cavity width, of 400 for two degrees of non-orthogonality, namely $\beta = 60°$ and 45°. These results were obtained on a 22 × 22 grid. It is seen that at a given Reynolds number the mesh skewness does not affect the convergence behaviour significantly. The coupled approach requires fewer iterations for convergence than the sequential approach.

The convergence histories at a Reynolds number of 1000 on a 22 × 22 grid are presented in Figure 5. Owing to the increased non-linearities at higher Reynolds numbers, the number of iterations needed for convergence is expected to increase. This is clearly seen in the results for

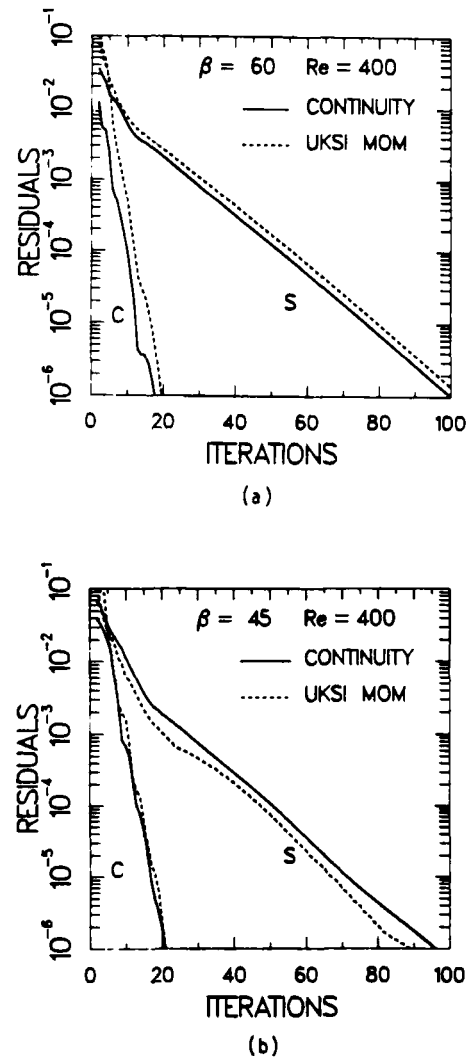


Figure 4. Convergence rates for the sheared cavity at $Re = 400$, 22 × 22 grid: (a) $\beta = 60°$; (b) $\beta = 45°$

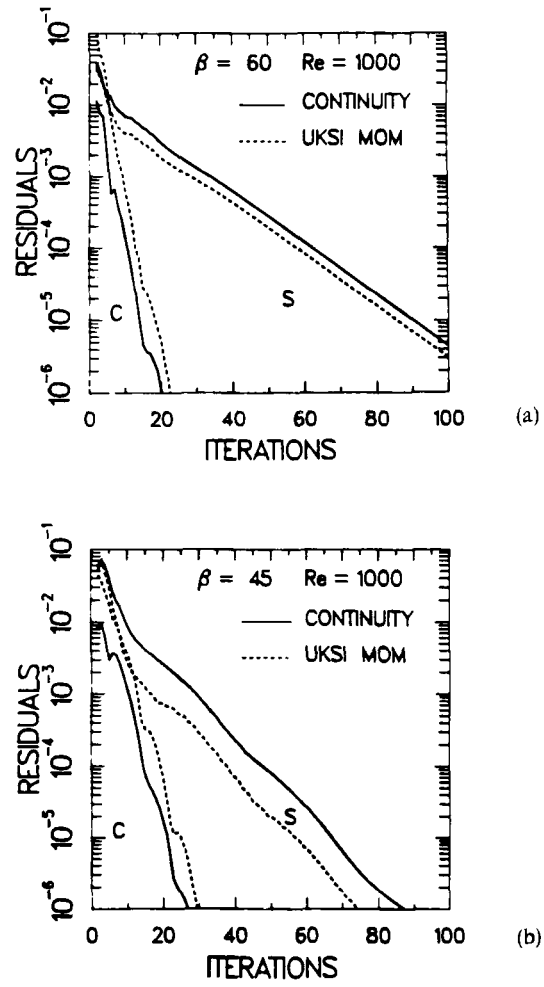


Figure 5. Convergence rates for sheared cavity at $Re = 1000$, 22 × 22 grid: (a) $\beta = 60°$; (b) $\beta = 45°$

$\beta = 60°$. The increase in the Reynolds number has a more pronounced effect on the performance of the sequential algorithm. In a sequential algorithm the cost of each iteration is nearly constant. Thus the overall cost varies linearly with the number of iterations. In the coupled algorithm the coefficient matrix is factorized only for the first few iterations and the subsequent iterations involve only forward and backward substitution. Therefore the additional iterations do not result in a proportional increase in the cost.

On a more non-orthogonal grid ($\beta = 45°$) an increase in the Reynolds number has a greater adverse effect on the performance of the coupled solution algorithm. The number of iterations needed for convergence is now larger in comparison with the $\beta = 60°$ case. This behaviour is attributed to the lack of a fully implicit treatment for all terms appearing in the continuity equation. An implicit treatment of the continuity would of course lead to a more robust algorithm. However, the presence of additional non-zero elements in the coefficient matrix causes a significant increase in the cost of LU decomposition. Consequently, the coupled solution

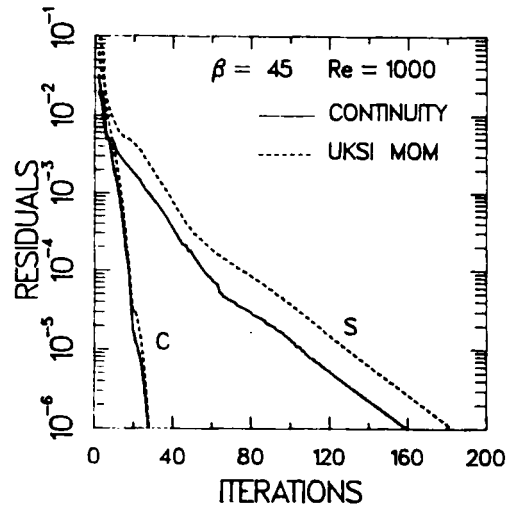


Figure 6. Convergence rates for sheared cavity at $Re = 1000$, 32 × 32 grid

algorithm no longer remains cost-effective. The trends seen in this test problem indicate that, on a given grid, the advantage of the coupled approach will diminish as the mesh skewness increases.

To study the effect of the number of grid points on the convergence rates, the $Re = 1000$, $\beta = 45°$ case was also run using a 32 × 32 uniformly spaced grid. The convergence rates on this grid are shown in Figure 6. By comparing these results with those corresponding to the 22 × 22 grid, it is seen that the coupled approach requires nearly the same number of iterations on both grids. This mild sensitivity to the number of grid points is an attractive feature of the coupled approach.

The results for $\beta = 45°$ on the two grids considered here indicate that even though the performance of the coupled algorithm deteriorates on highly non-orthogonal grids, it is still more efficient than the sequential algorithm since the latter approach requires a large number of iterations to achieve convergence. The relative advantage of the coupled procedure is expected to become more pronounced as the number of grid points is increased.

The computed flow fields, as depicted by the streamlines, at $Re = 1000$ for the two sheared cavities considered are shown in Figure 7. These indicate the flow development as a square cavity is gradually sheared.

*Planar curved channel*

This series of test problems is identical to that used in Reference 10. The results for cavity flow indicated that the use of a simple sheared grid similar to that employed in Reference 10 for the most skewed channel ($B = 2{\cdot}2$) will lead to convergence difficulties for the coupled algorithm. Consequently, only two configurations corresponding to $B = 0{\cdot}8$ and $1{\cdot}1$ have been selected. Results have been presented for a Reynolds number, based on the inlet height, of 2000. These flows are non-separating.

Figure 8(a) presents the convergence rates for the channel corresponding to $B = 0{\cdot}8$ using the 27 × 22 sheared grid shown in Figure 3(b). Similar to the findings for the sheared cavity, the coupled method converges faster.

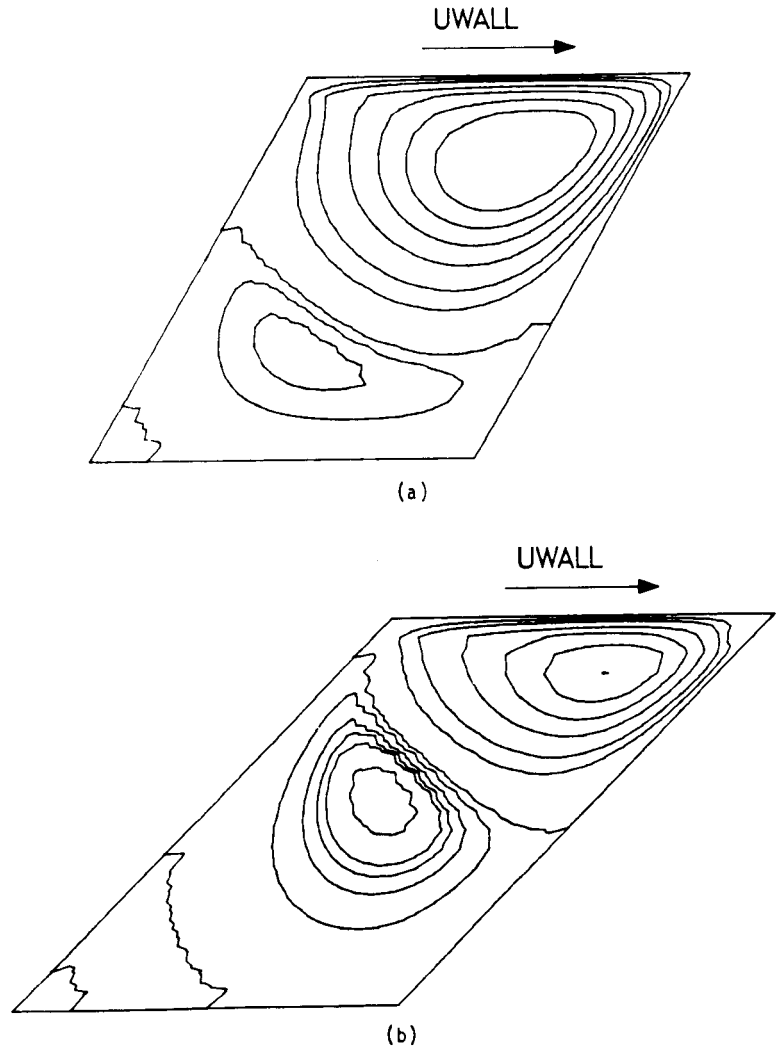


Figure 7. Computed flow fields for sheared cavity, Re = 1000: (a) $\beta = 60°$; (b) $\beta = 45°$

For this problem the convergence rate of the coupled algorithm is comparable to that observed for the sheared cavity with $\beta = 45°$. The performance of the sequential approach, however, is superior for the channel flow. An additional feature in these calculations is the presence of source terms in the momentum equations arising from the curvature of the grid lines. These terms are evaluated explicitly.

Owing to the relatively small difference between the number of iterations needed for convergence in the two approaches, the coupled procedure now requires more computational effort.

The convergence rates for the more skewed channel, corresponding to $B = 1{\cdot}1$, on a $27 \times 22$ grid are shown in Figure 8(b). Contrary to the results presented so far, the coupled method now requires more iterations for convergence than the sequential method. On the basis of the earlier discussion on the sheared cavity corresponding to $\beta = 45°$ and considering the non-orthogonality of the grid used here (Figure 3(c)), these results are not totally unexpected. Even though the flow

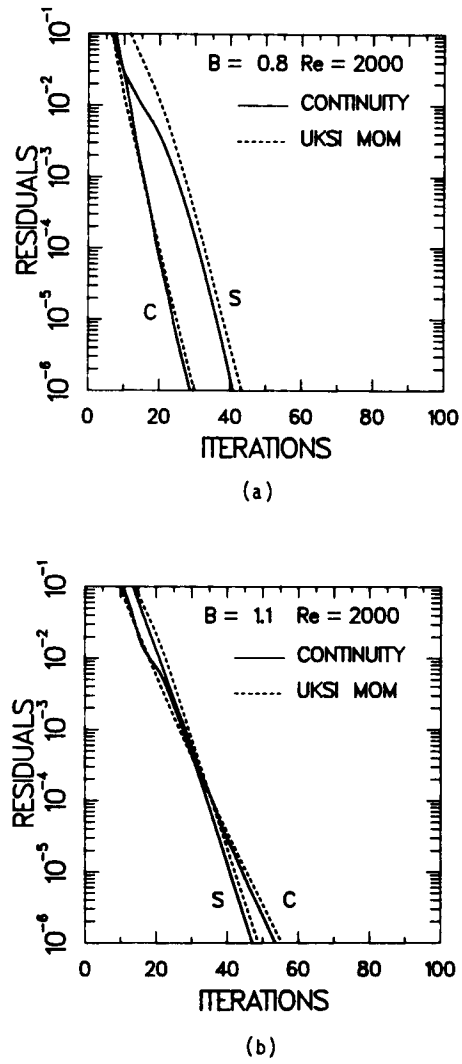


Figure 8. Convergence rates for the planar channel, 27 × 22 sheared grids shown in Figure 3: (a) $B = 0{\cdot}8$; (b) $B = 1{\cdot}1$

under consideration is simple, the grid skewness necessitates a fully implicit treatment of the continuity equation.

The results for the test cases considered in this study indicate that the coupled algorithm performs satisfactorily as long as the angles between the intersecting co-ordinate lines are greater than 45°.

For curved channel flows the coupled solution approach does not offer a significant advantage over the sequential approach, especially on highly non-orthogonal grids. In the comparative evaluation of these alternative solution procedures, some additional factors should also be included. First, if the performance of the sequential approach deteriorates considerably as the number of grid points is increased, the coupled algorithm should again become competitive on finer grids. Secondly, in many situations it is possible to generate grids which do not deviate as

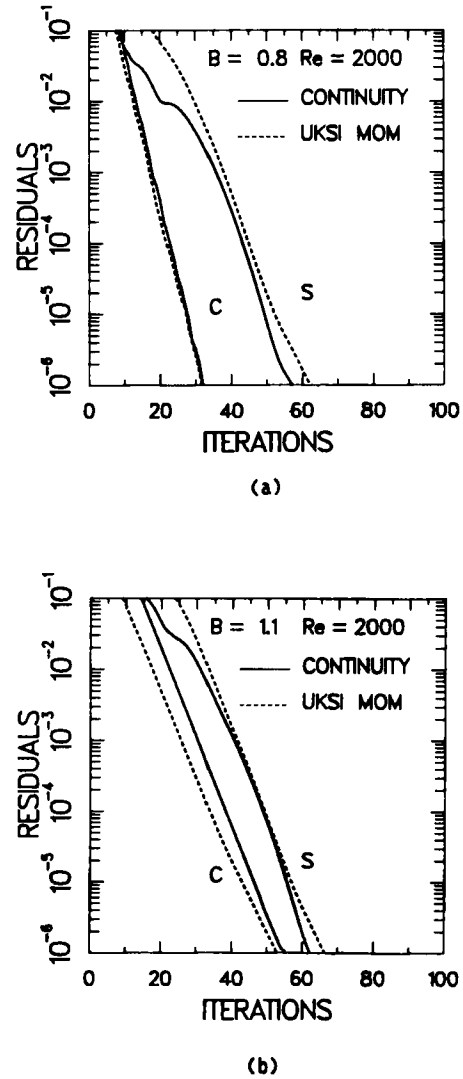


Figure 9. Convergence rates for the planar channel, 42 × 22 sheared grid: (a) $B = 0{\cdot}8$; (b) $B = 1{\cdot}1$

severely from orthogonality as the ones used here. Mild non-orthogonality is also desirable from the accuracy point of view. Again, the coupled solution procedure will be more efficient for such grids.

To demonstrate the effect of grid size, computations for the two channel configurations were repeated on 42 × 42 sheared grids. The convergence rates for the two algorithms are shown in Figure 9. The effect of grid refinement is very similar to that noticed for the sheared cavity. Again, the number of iterations needed by the coupled procedure is nearly independent of the grid size.

The calculations for the $B = 1{\cdot}1$ channel were also performed using the modified 42 × 22 grid shown in Figure 10. This grid represents an improvement over the sheared grid used earlier. Like all other grids used in this study, this grid was also generated algebraically. Figure 11 presents the

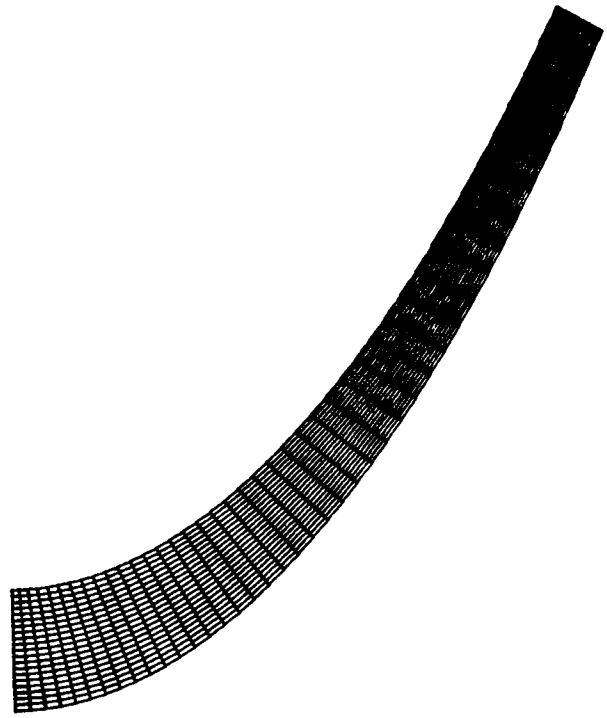

Figure 10. Modified grid for planar channel corresponding to $B = 1{\cdot}1$

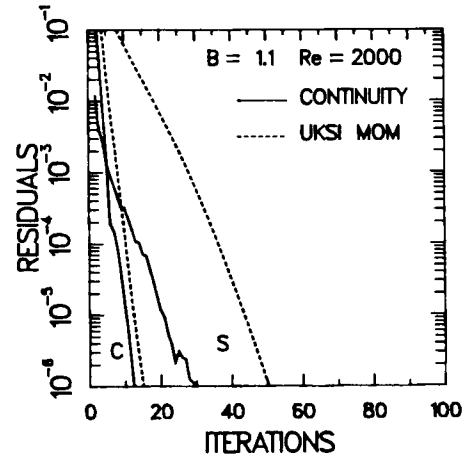


Figure 11. Convergence rates for the planar channel using the 42 × 22 grid shown in Figure 10

convergence behaviour for this test case. As expected, the performance of the coupled algorithm improves considerably on this grid.

A comparison of the present results for the channel flow cases ($B = 0{\cdot}8$ and $1{\cdot}1$) with those reported in Reference 10 indicates that for the sheared grids (Figures 3(b) and 3(c)) the number of iterations required for convergence by the coupled solution scheme is nearly the same for the two

Table II. Execution times (CRAY XMP CPU seconds)

| Test case | Sequential | Coupled |
|---|---|---|
| 1 | 7·54 | 4·03 |
| 2 | 6·56 | 3·87 |
| 3 | 8·63 | 4·44 |
| 4 | 7·26 | 6·65 |
| 5 | 37·38 | 20·84 |
| 6 | 3·80 | 4·10 |
| 7 | 4·21 | 6·20 |
| 8 | 8·65 | 7·89 |
| 9 | 9·10 | 11·50 |
| 10 | 9·20 | 6·05 |

formulations. However, since the present formulation results in fewer non-zero elements in the coefficient matrix, it should be less expensive. Part of the advantage would of course be offset by the need to calculate the curvature terms, which are treated in an explicit manner, as well as the need to solve for an additional pressure correction equation.

The relative performances of the sequential and the coupled algorithms for the present covariant velocity formulation and the Cartesian velocity formulation of Reference 10 should be assessed with caution. In the present study the velocity–pressure coupling in the sequential algorithm is handled via the SIMPLER algorithm whereas the SIMPLE algorithm was used in Reference 10. In earlier studies[8] the SIMPLER algorithm has been shown to be much superior to the SIMPLE algorithm for fluid flow calculations in Cartesian co-ordinates. Such a comparative study cannot be made on the basis of the results of this investigation and those of Reference 10 owing to major differences with regard to the choice of primary variables in the two formulations. Further, the performance of the sequential solvers depends on a proper choice of the under-relaxation factors and no attempt has been made to optimize these in either study.

## CPU TIME COMPARISON

The execution times (CRAY XMP CPU seconds) for the coupled and the SIMPLER-based sequential algorithms for the test cases considered are presented in Table II.

In previous studies,[8, 9] restricted to Cartesian co-ordinates, the coupled solution approach was shown to be two to three times faster than the SIMPLER algorithm. The present results indicate that for non-orthogonal grids with reasonable departure from orthogonality the coupled algorithm reduces the execution times by a factor of about two. For severely non-orthogonal grids the performance of the coupled algorithm deteriorates and it no longer remains cost-effective.

## CONCLUDING REMARKS

In this paper the implications of a coupled solution algorithm in conjunction with a curvilinear velocity formulation for fluid flow calculations in body-fitted co-ordinates were addressed. In the present formulation the structure of the coefficient matrix is kept identical to that in Cartesian co-ordinates. The additional terms resulting from the grid non-orthogonality and the use of curvilinear velocities inthe momentum equations were treated explicitly. Results indicate that

such a mixed treatment leads to an algorithm which can be used with advantage for reasonably non-orthogonal grids. However, the potential of the algorithm with regard to robustness cannot be fully realized, especially when the grid is highly skewed.

## REFERENCES

1. S. V. Patankar and D. B. Spalding, 'A calculation procedure for heat, mass, and momentum transfer in three-dimensional parabolic flows', *Int. J. Heat Mass Transfer*, **15**, 1787–1806 (1972).
2. S. V. Patankar, *Numerical Heat Transfer and Fluid Flow*, Hemisphere, Washington, D.C., 1980.
3. S. V. Patankar, 'A calculation procedure for two-dimensional elliptic flows', *Numer. Heat Transfer*, **4**, 409–425 (1981).
4. J. P. Van Doormal and G. D. Raithby, 'Enhancement of the SIMPLE method for predicting incompressible fluid flows', *Numer. Heat Transfer*, **7**, 147–163 (1984).
5. R. I. Issa, 'Solution of the implicitly discretized fluid flow equations by operator-splitting', *J. Comput. Phys.*, **62**, 40–65 (1986).
6. S. P. Vanka and G. K. Leaf, 'Fully-coupled solution of pressure-linked fluid flow equations', *ANL-83-73*, Argonne National Laboratory, IL, 1983.
7. S. P. Vanka, 'Block implicit calculation of steady turbulent recirculating flows', *Int. J. Heat Mass Transfer*, **28**, 2093–2103 (1985).
8. M. E. Braaten, 'Development and evaluation of iterative and direct methods for the solution of the equations governing recirculating flows', *Ph.D. Thesis*, University of Minnesota,1985.
9. S. V. Patankar, K. C. Karki and H. C. Mongia, 'Development and evaluation of improved numerical schemes for recirculating flows', *AIAA-87-0061*, 1987.
10. M. E. Braaten and W. Shyy, 'Comparison of iterative and direct solution methods for viscous flows in body-fitted coordinates', *Int. j. numer. methods fluids*, **6**, 325–349 (1986).
11. K. C. Karki, 'A calculation procedure for viscous flows at all speeds in complex geometries', *Ph.D. Thesis*, University of Minnesota, 1986.
12. K. C. Karki and S. V. Patankar, 'A calculation procedure for viscous incompressible flows in complex geometries', *Numer. Heat Transfer*, **14**, 295–307 (1988).
13. S. C. Einsentat, M. C. Gursky, M. H. Shultz and A. H. Sherman, 'Yale Sparse Matrix Package, II. The non-symmetric codes', *Research Report Number 114*, Department of Computer Sciences, Yale University, 1977.